Structure
Article

The Human Formin FHOD1 Contains a Bipartite Structure of FH3 and GTPase-Binding Domains Required for Activation

Antje Schulte,[1] Bettina Stolp,[2] André Schönichen,[1] Olena Pylypenko,[1] Alexey Rak,[1] Oliver T. Fackler,[2] and Matthias Geyer[1,*]
[1]Abteilung Physikalische Biochemie, Max-Planck-Institut für Molekulare Physiologie, Otto-Hahn-Strasse 11, 44227 Dortmund, Germany
[2]Abteilung Virologie, Universitätsklinikum Heidelberg, Im Neuenheimer Feld 324, 69120 Heidelberg, Germany
*Correspondence: matthias.geyer@mpi-dortmund.mpg.de
DOI 10.1016/j.str.2008.06.008

SUMMARY

Formins induce the nucleation and polymerization of unbranched actin filaments. They share three homology domains required for profilin binding, actin polymerization, and regulation. Diaphanous-related formins (DRFs) are activated by GTPases of the Rho/Rac family, whose interaction with the N-terminal formin domain is thought to displace a C-terminal Diaphanous-autoregulatory domain (DAD). We have determined the structure of the N-terminal domains of FHOD1 consisting of a GTPase-binding domain (GBD) and the DAD-recognition domain FH3. In contrast to the formin mDia1, the FHOD1-GBD reveals a ubiquitin superfold as found similarly in c-Raf1 or PI3 kinase. This GBD is recruited by Rac and Ras GTPases in cells and plays an essential role for FHOD1-mediated actin remodeling. The FHOD1-FH3 domain is composed of five armadillo repeats, similarly to other formins. Mutation of one residue in the predicted DAD-interaction surface efficiently activates FHOD1 in cells. These results demonstrate that DRFs have evolved different molecular solutions to govern their autoregulation and GTPase specificity.

INTRODUCTION

Formin homology proteins play crucial roles in the reorganization of the actin cytoskeleton to modulate various functions of the cell cortex including motility, adhesion, and cytokinesis (Pantaloni et al., 2001; Pollard and Borisy, 2003; Goode and Eck, 2007). They are multidomain proteins of typically more than 120 kDa molecular weight that interact with cytoskeletal proteins and diverse signaling molecules to transmit extracellular stimuli toward actin nucleation and polymerization. The polar structures of actin filaments are characterized by a fast-growing barbed and a slow-growing pointed end. Formins promote F-actin assembly at the filament barbed end and move processively with the barbed end as it elongates (Pruyne et al., 2002; Sagot et al., 2002; Higashida et al., 2004). Based on their ability to act as potent nucleators of actin polymerization, formins were found to be involved in the formation of actin cables in yeast and stress fibers in mammalian cells, the assembly of contractile rings during cytokinesis, and the formation of filopodia (Faix and Grosse, 2006; Goode and Eck, 2007).

Formins are characterized by the presence of a conserved formin homology 2 (FH2) domain of about 400 amino acids in length (Wallar and Alberts, 2003; Evangelista et al., 2003). This domain forms the catalytic unit for the nucleation of actin polymers in vivo, and for some formins the sole FH2 domain is already sufficient to nucleate actin polymerization from G-actin in vitro (Watanabe et al., 1999; Pruyne et al., 2002; Sagot et al., 2002). The FH2 domain is in most formins accompanied by an N-terminal proline-rich FH1 domain that is required for profilin binding (Romero et al., 2004) but may also interact with Src-homology 3 (SH3) or WW domains. The length of this stretch and the number of prolines within is thought to directly correlate to the actin polymerization kinetics of the formin (Vavylonis et al., 2006). The structurally and functionally least-conserved module is the N-terminal FH3 domain, which has been implicated in subcellular localization and formin regulation (Petersen et al., 1998; Kato et al., 2001; Ozaki-Kuroda et al., 2001; Seth et al., 2006; Brandt et al., 2007). Based on these three homology regions, phylogenetic analysis defined seven subfamilies of formins: Diaphanous (Dia), dishevelled-associated activator of morphogenesis (DAAM), formin-related gene in leukocytes (FRL; also named formin in leukocytes [FMNL]), formin homology domain-containing protein (FHOD), inverted formin (INF), formin/Cappucino (FMN), and delphilin (Higgs and Peterson, 2005; Rivero et al., 2005).

The modular architecture of formins varies throughout the different subfamilies and is combined with increased signaling complexity due to an array of additional regulatory domains (Wallar and Alberts, 2003; Faix and Grosse, 2006). A subset of formins that act as effectors of GTP-binding proteins of the Rho/Rac family is known as Diaphanous-related formins (DRFs). In DRFs, the FH1 and FH2 domains are flanked by a C-terminal Diaphanous-autoregulatory domain (DAD) and an N-terminal GTPase-binding domain (GBD) (Watanabe et al., 1999; Alberts, 2001). In the absence of an activating signal, DRFs are held in an inactive autoinhibited conformation by the interaction between the DAD and the N-terminal regulatory region. Deletion of the DAD results in constitutively active formins as shown, for example, for mDia1, Bni1, and FHOD1 (Watanabe et al., 1999; Ishizaki et al., 2001; Gasteier et al., 2003). The autoinhibition is relieved at least in part by binding of an activated GTPase to the regulatory region.

Structural studies have recently begun to complement the functional analyses of formins. Crystal structures of the FH2 domains from the yeast formin Bni1 and human DAAM1 showed that the all-helical FH2 domain forms a head-to-tail dimer tethered together by an N-terminal linker (Xu et al., 2004; Otomo et al., 2005a; Lu et al., 2007). The FH2 dimer contacts three actin molecules, which allows for interconversion between polymerization and depolymerization to suggest a stair-step mechanism of processive elongation at the barbed end (Otomo et al., 2005a). Deletion of the flexible linker converts the FH2 domain from an inducer of actin polymerization to an inhibitor, as shown for the FH2 domain of mDia1 (Shimada et al., 2004). Also, the N-terminal domain structure of the DRF mDia1 was solved by X-ray crystallography alone, in complex with the GTPase RhoC and in complex with a fragment of the DAD-autoregulatory motif (Otomo et al., 2005b; Rose et al., 2005; Lammers et al., 2005; Nezami et al., 2006). Together, these structures encompass residues 69–451 of mDia1, revealing that the all-helical structure consists of three subdomains: a short Rho-binding segment of three twisted helices, an armadillo repeat region that is required for the recognition of the DAD, and a C-terminal dimerization domain. The MDxLL consensus motif of the DAD folds as a helix in the concave site of the armadillo repeat structure (Lammers et al., 2005; Nezami et al., 2006). Surprisingly, the DAD and the GTPase binding sites on this protein surface were not overlapping, suggesting that the mutually exclusive binding of Rho and DAD is not simply due to a steric displacement (Otomo et al., 2005b; Rose et al., 2005; Lammers et al., 2005).

The ubiquitously expressed human DRF FHOD1 shares with other DRF family members the characteristic FH1, FH2, and DAD domains, the ability to form FH2 multimers, and DAD-mediated autoregulation (Westendorf et al., 1999; Gasteier et al., 2003; Takeya and Sumimoto, 2003; Koka et al., 2003; Madrid et al., 2005; Schönichen et al., 2006). The N-terminal region (1–573), however, differs significantly in sequence from other DRFs, and structure prediction fails to identify the GBD and FH3 domains. Also, in contrast to most other DRFs, FHOD1 interacts with Rac and not Rho or Cdc42 GTPases (Westendorf, 2001; Gasteier et al., 2003). Truncation of its DAD results in a deregulated, constitutively active FHOD1 variant that potently induces the formation of thick F-actin bundles and triggers transcription from the serum response element (SRE) (Gasteier et al., 2003). The phenotype of thick actin stress fibers is, however, not induced upon coexpression of active Rac with the full-length FHOD1 DRF.

To understand the molecular basis of its autoregulation and GTPase interaction, we determined the crystal structure of the N-terminal domains of human FHOD1. The structure of the FH3 domain is composed of five armadillo repeats and shows similarity to the corresponding domain of mDia1. Disruption of the DAD-interaction surface by a single point mutation in the FH3 domain potently activates FHOD1 in cells. Surprisingly, the N-terminal GBD exhibits structural similarity to the ubiquitin superfold as found, for example, in the Ras-binding domains of c-Raf1 or PI3 kinase, but contains an unusual loop that inserts into the first FH3 repeat. This GBD is essential for FHOD1 activities in actin remodeling and transcriptional activation, localizes to specific GTPases in cells, and binds to GTPases in vitro.

RESULTS

Structure Determination of the N-Terminal Domains of Human FHOD1

The sequence homology between FHOD1 and other formins of the DRF family is not sufficient to reliably determine boundaries of functional domains in the N-terminal region preceding the FH1 section. Knowledge of the structure of N-terminal domains in mDia1 (Rose et al., 2005; Otomo et al., 2005b) could thus not be transposed to FHOD1 for the generation of functional units. We previously identified fragment 1–377 of FHOD1 as sufficient for DAD binding (Schönichen et al., 2006). Initial crystallization trials using this construct resulted in crystals that diffracted to a 3.8 Å resolution but resisted further improvements. Subsequently, FHOD1 fragments starting with residues 1, 10, 52, or 78 and C-terminal boundaries 339, 357, 369, or 377 were generated (see Figure S1 available online). Whereas the two capacious N-terminal truncations resulted in insoluble proteins, all C-terminal truncations yielded soluble and stable protein products. In the following, construct 1–339 is referred to as $FHOD1_N$ (Figure 1A). Size-exclusion chromatography showed reversible dimerization of this fragment due to disulfide bonding. Thus, a number of cysteine-to-serine mutations were generated in different combinations. Whereas mutation of C43, C164, or C211 yielded unstable proteins, the double mutation C31S, C71S remained monomeric even upon long-term exposure at oxidative conditions.

Crystals of $FHOD1_N$ (C31S, C71S) were grown using the hanging-drop vapor-diffusion technique as described (Schulte et al., 2007). Since no molecular replacement solution using the FH3 domain 135–369 of mDia1 (Rose et al., 2005) or a fragment consisting of three to five armadillo repeats of Importin α (Conti et al., 1998) could be found for a native data set, selenomethionine (SeMet) crystals of $FHOD1_N$ were grown that diffracted to 2.9 Å resolution. The structure was solved by the method of multiwavelength anomalous dispersion (MAD) with the SeMet derivative. The structure of $FHOD1_N$ was refined at 2.3 Å resolution to a crystallographic R value of 21.9% and a free R value of 25.9% with good stereochemistry (Table 1). There are two independent molecules in the asymmetric unit of the crystals (chains A and B) that contact each other in one surface spot between the C terminus of molecule A and the N terminus of molecule B (Figure 1B). The model discussed in the text includes residues 14–339 with the exception of a short disordered loop region (residues 95–96 in model A and 93–107 in model B, respectively), with almost 93% of the residues lying in the most favored regions of the Ramachandran plot (Table 1). As the site chain density of model A was better defined in the crystal, the latter will be used for further analysis.

The overall structure of $FHOD1_N$ consists of two units, a compact N-terminal α/β roll structure and a succeeding armadillo repeat fold (Figures 1B and 1C, displayed in green and blue, respectively), assembled to form an elongated molecule. Both domains are tightly linked by one residue, Q115, that connects the C-terminal β strand of the first domain to the first α helix of the second domain. Superposition of the $FHOD1_N$ structure with mDia1 69–451 (Rose et al., 2005) confirms the presence of an armadillo repeat fold in formins despite low sequence homology (Figure 1D). This domain, which

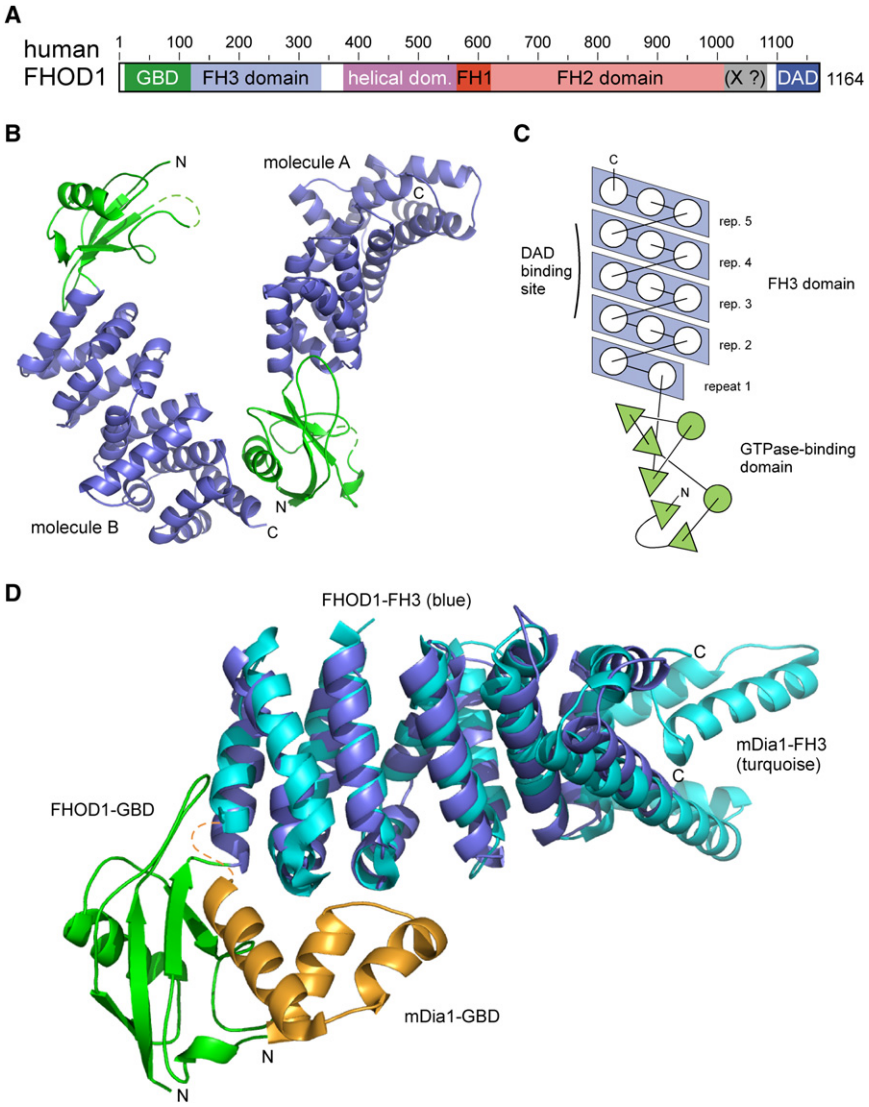

Figure 1. Overall Domain Architecture of FHOD1 and Structure of Its N-Terminal Domains

(A) Proposed domain organization of human FHOD1. The schematic drawing of the 125 kDa protein encodes an N-terminal GTPase-binding domain (GBD), the DAD-recognition domain FH3, a proposed helical region of yet unknown function, the proline-rich FH1 domain, the catalytic FH2 domain, an FHOD-specific segment of approximately 80 residues (X), and the C-terminal Diaphanous-autoregulatory domain (DAD).

(B) Structure of the N-terminal GBD and FH3 domains of FHOD1 14–339. Two molecules in the asymmetric unit contact each other in one surface spot between the N terminus of molecule A and the C terminus of molecule B.

(C) Topology diagram of the N-terminal domains including the proposed DAD interaction site.

(D) Superimposition of the N-terminal domains of FHOD1 (14–339; Protein Data Bank [PDB] ID code 3DAD) and mDia1 (69–451; PDB ID code 1Z2C). Whereas the armadillo repeat structure of the FH3 domain is conserved in both proteins despite no primary sequence similarity, the GBD structure is different in the two DRFs.

is also called Diaphanous-inhibitory domain (DID; Li and Higgs, 2005), was described first in the fission yeast formin Fus1 as a functional unit with a repetitive structure (Petersen et al., 1998). Following the protein family database (PFAM accession number PF06367), we thus identify residues 115–339 as the FH3 domain of FHOD1. In contrast, the N-terminal domain structure differs significantly from the mDia1-GBD fold (Figure 1D).

The FH3 Domain Adopts a Conserved Armadillo Repeat Structure

The FH3 domain 115–339 of FHOD1 is composed of a repetitive bundle of 14 α helices, which are assembled by an initiating HEAT repeat followed by four canonical armadillo repeats, each stacked together to form an elongated superhelical domain (Figure 2A). The individual repeats vary significantly in their sequence length, ranging from 36 residues for the first repeat to 55 residues in the fourth repeat (Figure 2B). The variation in repeat length might be one reason why the armadillo repeat composition is not predicted by automated domain-recognition analysis. The third helices (H3), which compose the concave surface of the armadillo repeat fold, however, are very similar in length and correlate accurately to the consensus sequence of armadillo repeats (Andrade et al., 2001). Moreover, these helices are particularly well conserved within the FHOD formin family, as can be seen from a sequence alignment plotted against the secondary structure elements (Figure S2, helices α4, α7, α10, and α13). The C-terminal armadillo repeat finally is clearly marked off from a succeeding repeat by the presence of polar residues D307, E331, and K335 instead of leucines (at positions 10, 32, and 36 of the representative consensus fold) that otherwise define the hydrophobic connecting points to the flanking helices. Superposition of FHOD1-FH3 115–339 with the respective section 135–369 of murine mDia1 (Rose et al., 2005) reveals a root-mean-square deviation (rmsd) value of 2.4 Å over a number of 208 Cα atoms, sharing 19.2% sequence identity. In contrast, the helices on the concave site of the first four repeats overlap with an rmsd value of 1.4 Å over 58 Cα atoms, indicating the homogeneity and structural conservation of this domain. A structure-based sequence alignment between the two domains is shown in Figure S3.

Mutation of a Single Residue in the FH3 Domain Results in FHOD1 Activation

Despite intensive screening, we did not succeed in cocrystallizing $FHOD1_N$ with the DAD or in soaking peptides of various lengths containing the DAD-interaction motif into the crystals. Because residues that critically mediate the autoinhibitory

Table 1. Structure Refinement Statistics	
Resolution of native FHOD1$_N$ (Å)	19.6–2.3
Resolution of selenomethionine FHOD1$_N$ (Å)	19.9–2.9
Number of modeled amino acid residues	635
Number of water molecules	237
R_{work} (%)[a]	21.9
R_{free} (%)[b]	25.9
Rmsd from ideal geometry: bond lengths (Å)/angles (°)	0.0064/1.13
Average B factors (Å^2)	43
Ramachandran plot	
Most favored region (%)	92.9
Additional allowed region (%)	6.9
Generously allowed region (%)	0.2
Disallowed region (%)	0

[a] $R_{work} = \Sigma|F_o - F_c|/\Sigma F_o$, where F_o and F_c are the observed and calculated structure factor amplitudes, respectively.
[b] R_{free} was calculated similarly to R_{work} using the test set reflections.

FH3-DAD interaction have been described for mDia1 (Lammers et al., 2005; Nezami et al., 2006), the structural homology of the FH3 domain fold allowed us to extrapolate on analogous residues in FHOD1 (Figures 3A and 3B). Based on a domain superimposition, valine at position 228 was mutated to glutamate in FHOD1 to mimic the corresponding alanine 256-to-aspartate mutation in mDia1 (Lammers et al., 2005). Initial pull-down experiments were performed using GST-tagged FHOD1-DAD (1096–1164) for precipitation of wild-type or mutant FHOD1$_N$ protein. Although the wild-type protein was efficiently precipitated from solution similarly as described (Schönichen et al., 2006), mutation of V228E abrogated binding to the DAD in vitro (data not shown).

To test whether the reduced affinity between DAD and FH3 (V228E) also causes the release of autoinhibition in the context of full-length FHOD1, the biological activity of the V228E FHOD1 mutant was compared to full-length wt FHOD1 and two constitutively active FHOD1 variants that lack the DAD (1–1010) or carry mutations in the DAD motif (DR9), respectively (Gasteier et al., 2003; Schönichen et al., 2006; Westendorf, 2001; Koka et al., 2003). All proteins were expressed to comparable levels in NIH 3T3 cells (Figure 3E). The induction of thick F-actin bundles as well as enhanced transcription from a luciferase reporter plasmid under the control of the SRE were employed as standard assays for FHOD1's biological activity (Gasteier et al., 2003). Expectedly, expression of wt FHOD1 did not induce marked actin reorganization or SRE transcription, whereas the deregulated DR9 and the more potent 1–1010 FHOD1 variants were active in both assays (Figures 3C and 3D). Importantly, the V228E FHOD1 mutant induced formation of thick actin bundles as well as SRE transcription with efficiencies at least comparable to that of FHOD1 1–1010. Thus, V228 critically determines the DAD-FH3 interaction in full-length FHOD1, and disruption of this autoinhibition activates the DRF in cells, suggesting a similar structural basis as determined for mDia1. The DAD-FH3 autoregulatory interaction therefore appears as a highly conserved mode of regulation in DRFs.

The FHOD1-GBD Shows Similarities to the Ras-Binding Domain of Raf

The structure of the N-terminal domain 14–115 of FHOD1 contains a five-stranded mixed β sheet packed against an α helix with a short helix prior to strand 5 (Figure 4A). The first two strands

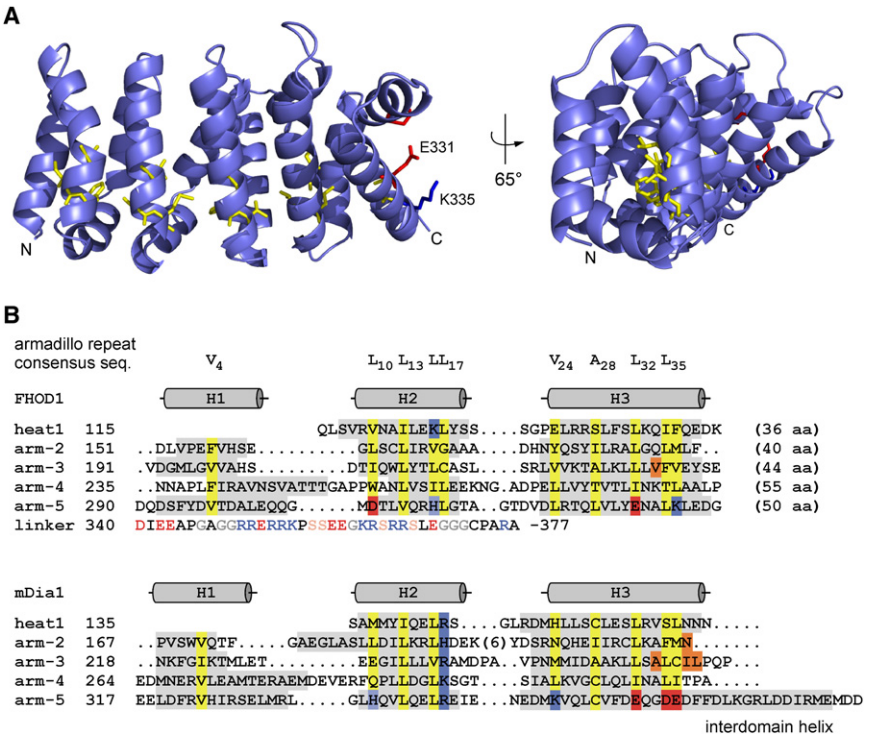

Figure 2. Structure of the FHOD1-FH3 Domain

(A) The elongated structure is composed of five armadillo repeats with hydrophobic interactions connecting the individual segments.

(B) Sequence conservation and secondary structure element comparison of the armadillo repeat structures in FHOD1 and mDia1 (PDB ID code 2BAP; Lammers et al., 2005). α helices are shaded gray. The armadillo repeat consensus sequence reported by Andrade et al. (2001) is printed at the top. Hydrophobic residues that mediate the core scaffold within the armadillo repeats are marked yellow. Positively and negatively charged residues in the fifth repeat that terminate the repetitive fold are labeled blue and red, respectively. Key residues for the interaction with the DAD consensus motif in the second and third repeats are labeled orange.

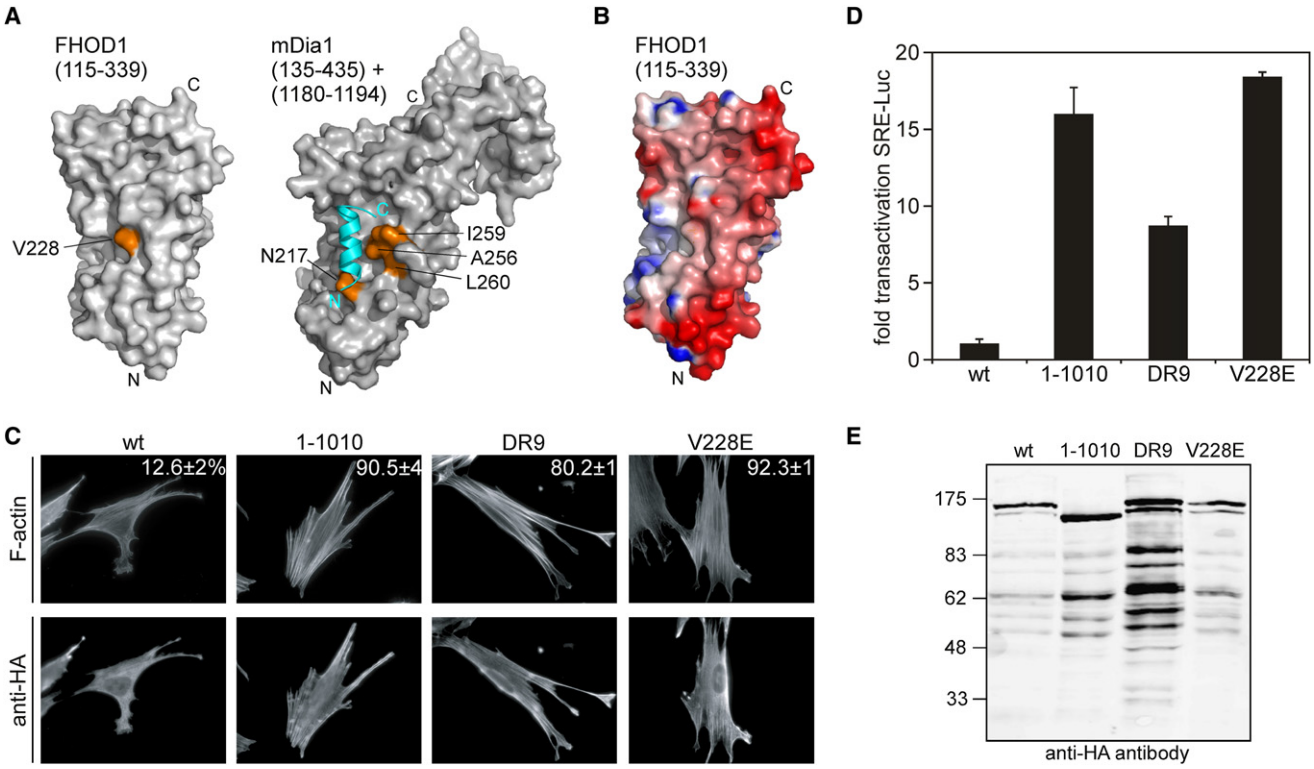

Figure 3. Activation of FHOD1 by Mutation of the DAD-Recognition Surface in the FH3 Domain

(A) Site-by-site display of V228 in the armadillo repeat structure of FHOD1 (left) and interacting residues N217, A256, I259, and L260 in the mDia1 FH3-DAD complex structure (right) (PDB ID code 2BAP; Lammers et al., 2005).

(B) Electrostatic surface potential of FHOD1-FH3 displayed from −12 k_BT (red) to +12 k_BT (blue). The large negatively charged patch may interact with the basic cluster of the DAD.

(C) Subcellular localization and F-actin organization of NIH 3T3 cells expressing the indicated HA-tagged FHOD1 variants. Following fixation, cells were stained for F-actin (upper panel) and HA-FHOD1 (lower panel) and analyzed by immunofluorescence microscopy. The numbers indicate the mean percentage with standard deviation of cells expressing the respective FHOD1 variant that displayed thick actin stress fibers in three independent experiments with at least 100 cells evaluated each.

(D) SRE luciferase reporter assay. Shown is the fold transactivation of the SRE luciferase reporter in NIH 3T3 cells expressing the indicated FHOD1 variants. Luciferase activity for FHOD1-wt expressing cells was arbitrarily set to 1. Presented are average values from one of at least three independent experiments with the indicated standard deviation from independent triplicates.

(E) Western blot analysis of the cells used in (C) and (D).

assemble in an antiparallel mode with a long loop of 18 residues (24–41) in between. The following three strands form a Greek key motif with the C-terminal strand oriented parallel to strand 1 to generate the full β sheet. This domain exhibits the ubiquitin superfold, which is a frequently occurring structural unit of high stability (Orengo et al., 1997). The hydrophobic core of the FHOD1 domain structure is formed by amino acids V20, P41, V58, L73, L82, and L110 that build one central layer assembled from residues of all five β strands and helix α1 (Figure 4A). The β sheet is twisted from the central strand β1 to the terminal strand β4 by more than 90°, thereby wrapping toward the N terminus of the long helix α1 due to the formation of hydrophobic contacts around L51. The loop between the first two β strands is well defined in the electron density map and connected to the succeeding FH3 domain by insertion of a conserved phenylalanine (F29) into a hydrophobic cleft of the first HEAT repeat (Figures 4B and 4C).

The ubiquitin superfold has been identified first as a GTPase-binding domain in the serine/threonine kinase c-Raf1, termed the Ras-binding domain (RBD; Nassar et al., 1995; Geyer and Wittinghofer, 1997). The complex of Raf-RBD with Rap1A showed the formation of an intermolecular β sheet between the terminal β2 strand of the RBD and the effector loop region (switch I) of the GTPase. Similarly, the GTPase-interacting regions of RalGDS, Byr2, and the phosphoinositide 3 kinase (PI3K) were found to comply with the ubiquitin superfold despite low sequence homology (Geyer et al., 1997; Huang et al., 1998; Vetter et al., 1999; Scheffzek et al., 2001, Pacold et al., 2000). Also, the FERM domain, which defines members of the band 4.1 superfamily, including cytoskeletal proteins such as the Ezrin-Radixin-Moesin (ERM) protein family, contains a structural module (named F1) that exhibits the ubiquitin superfold (Pearson et al., 2000). The conservation of the hydrophobic core constituents that determine this fold is revealed by a structure-based sequence alignment of FHOD1 14–115 compared to the GTPase-binding domains of Raf, RalGDS, Byr2, PI3Kγ, and those of Moesin and ubiquitin (Figure 4D). A search for structural homologs of the FHOD1-GBD using the DALI program (http://www.ebi.ac.uk/dali/) showed indeed highest similarity to RalGDS (Z score 9.3),

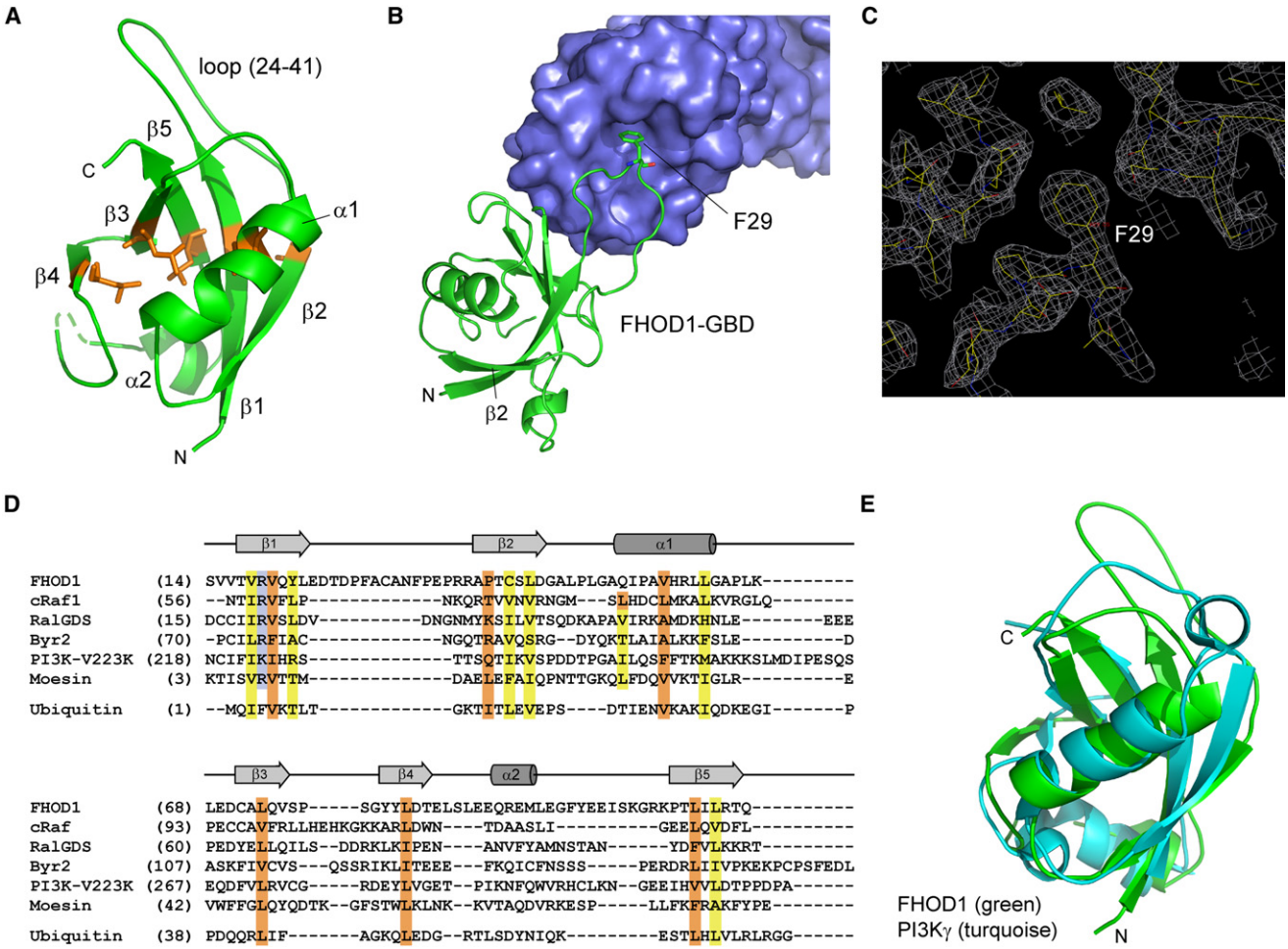

Figure 4. Structure of the FHOD1-GBD

(A) The ubiquitin fold of FHOD1 14–115 is defined by hydrophobic residues (labeled orange) that assemble to a core layer to form the β sheet structure.

(B) The GBD tightly interacts with the FH3 domain by its long loop between the first and second β strands. F29 inserts into a hydrophobic cleft of the first HEAT repeat composed of residues I123, K126, L127, L142, and I145.

(C) Electron density omit map of the GBD(F29)-FH3 interaction contoured at 1 σ.

(D) Structure-based sequence alignment of GTPase-binding domains that contain a ubiquitin superfold. The structures were superimposed using the Coot program, and aligned for the hydrophobic core residues labeled orange and yellow. FHOD1, as determined here, c-Raf1 (PDB ID code 1GUA; Nassar et al., 1995), RalGDS (PDB ID code 1LFD; Huang et al., 1998), Byr2 (PDB ID code 1K8R; Scheffzek et al., 2001), PI3K (PDB ID code 1HE8; Pacold et al., 2000), Moesin (PDB ID code 1EF1; Pearson et al., 2000).

(E) Superimposition of FHOD1-GBD 14–115 (green) with the RBD 218–312 of PI3Kγ (PDB ID code 1HE8; Pacold et al., 2000; turquoise) reveals an rmsd value of 2.5 Å over 81 Cα atoms.

followed by Moesin and PI3K. The length of the aligned sequences, however, is longest for the Ras-binding domain of PI3Kγ, with an rmsd value of 2.51 Å over 81 Cα atoms, as shown in the superposition of both domains (Figure 4E). The presence of an exposed basic residue (R19 in FHOD1) in the first β strand is thereby a specific feature of ubiquitin-like GBDs. These results suggested that the N terminus of FHOD1 comprises a GBD.

The FHOD1-GBD Is Essential for Its Biological Activity

We next asked whether the N-terminal GBD contributes to the biological activity of FHOD1 and performed functional analyses in NIH 3T3 cells analogous to those described above. Expression of the GBD alone or the GBD-FH3 fragment did not cause actin remodeling or SRE transcription (Figures 5A and 5B), and neither fragment displayed marked subcellular localization. Whereas these domains thus did not reveal any intrinsic biological activity, deletion of the N-terminal GBD from the active FHOD1 variant lacking the DAD 116–1010 resulted in a marked loss of activity in F-actin bundle formation and SRE transcription (compare 1–1010 and 116–1010 in Figures 5A and 5B). Also in contrast to the active FHOD1 variants, 116–1010 did not localize to F-actin-rich structures. Similar results were obtained when the 1–115 deletion was analyzed in the context of the DR9 mutant (data not shown). Finally, truncation of the GBD in the context of full-length FHOD1 116–1164 did not result in activation of the DRF. Expression levels are shown by western blot analysis (Figure 5C). We conclude that the N-terminal GBD plays a crucial role for the biological activity of the DRF in cells.

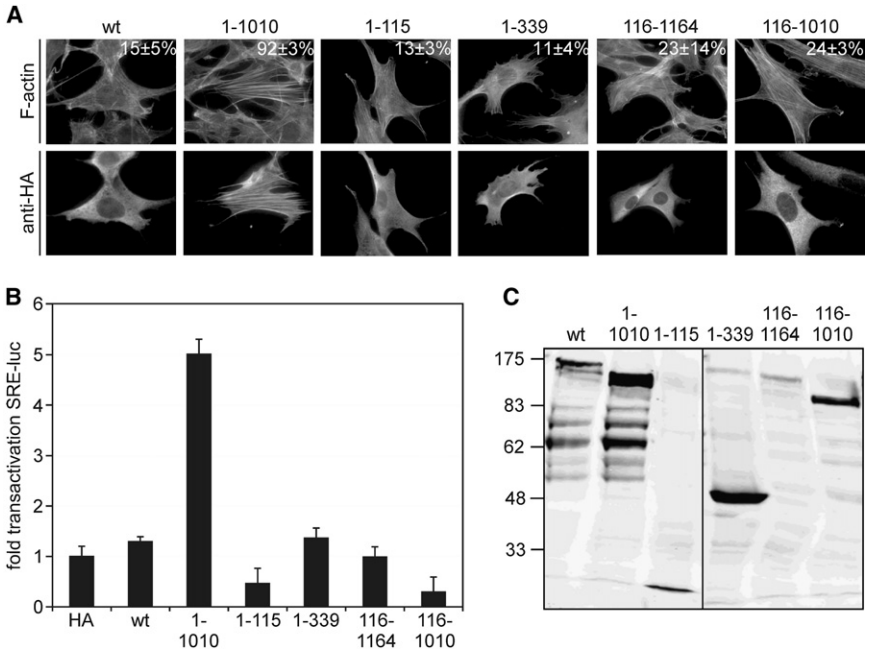

Figure 5. Functional Relevance of the N-Terminal FHOD1-GBD

(A) Subcellular localization and F-actin organization of NIH 3T3 cells expressing the indicated HA-tagged FHOD1 variants. Following fixation, the cells were stained for F-actin (upper panel) and HA-FHOD1 (lower panel) and analyzed by immunofluorescence microscopy. The numbers indicate the mean percentage with standard deviation of cells expressing the respective FHOD1 variant that displayed thick actin stress fibers. Three independent experiments with at least 100 cells were evaluated each.

(B) SRE luciferase reporter assay. Shown is the fold transactivation of the SRE luciferase reporter in NIH 3T3 cells expressing the indicated FHOD1 variants. Luciferase activity for FHOD1-wt expressing cells was arbitrarily set to 1. Presented are average values from one of at least three independent experiments with the indicated standard deviation from independent triplicates.

(C) Western blot analysis of the cells used in (A) and (B).

Interaction of the FHOD1-GBD with Rac and Ras GTPases

Although FHOD1 is supposed to associate with the Rac GTPase (Westendorf, 2001; Gasteier et al., 2003), no detailed information is available on the functional relevance of this interaction and on the protein surfaces involved. However, the subcellular localization of the DRF is markedly changed in the presence of activated Rac1, which triggers its recruitment to the plasma membrane (Gasteier et al., 2003). As the often-observed low affinity in the interaction of effector GBDs to GTPases precluded also for FHOD1 the direct identification of binding partners of its GBD by immunoprecipitation, we screened an array of GTPases for their ability to trigger relocalization of the FHOD1-GBD in cells. Active or wild-type variants of 33 GTPases of the Rho/Rac-, Ras-, and Ras-like GTPase families were expressed in NIH 3T3 cells together with the FHOD1-GBD. Distributed diffusely in the cytoplasm and the nucleus when expressed alone, the GBD showed a pronounced recruitment to the plasma membrane upon expression of active Rac1G12V, where it colocalized with the GTPase (Figure 6A). Similarly, efficient plasma membrane recruitment was also observed in the presence of active Rac2 and Rac3. These effects were specific, as most of the GTPases tested including, for example, active RhoA or active Cdc42 had no effect on GBD localization. Less efficient but appreciable recruitment was observed upon coexpression of the GBD with the placental Cdc42 isoform, Rnd1–3, TCL, as well as N-Ras and R-Ras (Figure 6B). These results demonstrate that the FHOD1-GBD is recruited by a specific set of GTPases in cells with the strongest response toward active Rac isoforms.

To analyze whether the colocalization experiments potentially reflect a direct GBD-GTPase interaction, in vitro binding studies were performed with H-Ras, Rnd3, TCL, RhoA, and Rac1 GTPases. GST pull-down experiments with GppNHp-activated GTPases fused to GST did not result in any detectable precipitation of either $FHOD1_N$ or FHOD1-GBD. Similarly, isothermal titration calorimetry (ITC) experiments failed to reliably observe a direct interaction (data not shown). Encouraged by a previous study on the PI3Kγ effector interaction where a single point mutation of V223 to lysine resulted in stable complex formation with Ras (Pacold et al., 2000), we thus searched for potential key residues that might influence the effector-GTPase interaction. Based on structural data of the complexes of Ras with Raf (Nassar et al., 1995), RalGDS (Huang et al., 1998; Vetter et al., 1999), Byr2 (Scheffzek et al., 2001), and PI3K (Pacold et al., 2000), as well as on the comprehensive literature governing the field of GTPase-effector recognition (Herrmann, 2003; Wohlgemuth et al., 2005; Kiel and Serrano, 2006), we identified four positions in FHOD1-GBD that might act as "hotspots" for GTPase interaction. Point mutations P41K, D46R, L61K, and T109R were introduced individually in $FHOD1_N$ and FHOD1-GBD plasmids. Whereas T109R yielded unstable protein, the remaining three mutations were tested in ITC experiments for their interaction with Ras and Rac GTPases. Changes in the heat disposal curve were indeed observed for FHOD1-GBD (P41K) with activated GST-Ras(1–189)•GppNHp, indicating a direct interaction (Figure 6C). In contrast, inactive GST-Ras(1–189)•GDP did not result in binding to FHOD1 (Figure 6D), supporting the specificity in effector recognition. The two other mutations, D46R and L61K, instead did not result in detectable binding (data not shown). Together, these results suggested that the FHOD1-GBD directly links the DRF to GTPases with select specificity.

DISCUSSION

In this study, we determined the crystal structure of the N-terminal GTPase-binding and FH3 domains of human FHOD1. Surprisingly, the GBD exhibits structural similarities to known GTPase effector domains such as in c-Raf1, RalGDS, PI3 kinase, or the Ezrin-Radixin-Moesin family. This result is unexpected, and protein domain analysis may have failed to identify this

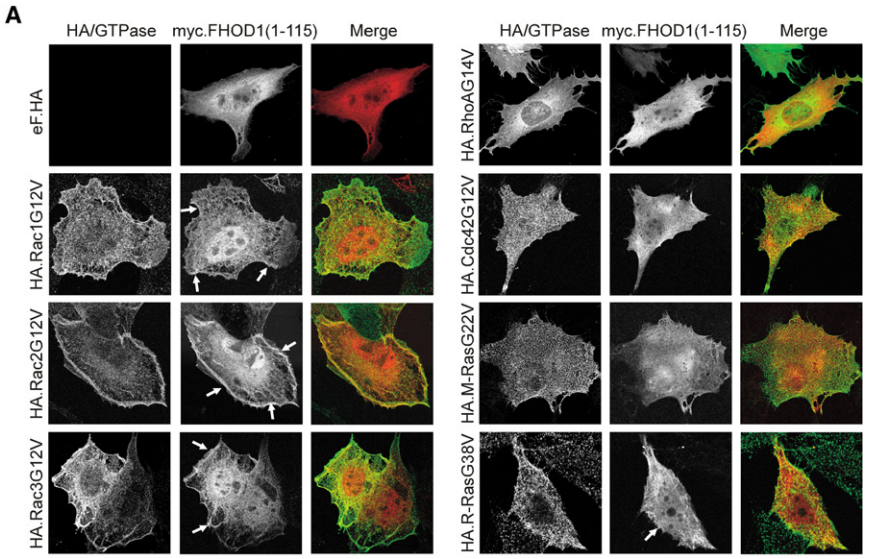

Figure 6. Interaction of the FHOD1-GBD with GTPases

(A) Confocal microscopic analysis of relocalization of the FHOD1-GBD by specific GTPases. Shown are representative pictures of NIH 3T3 cells expressing myc-tagged FHOD1 1–115 and the indicated HA-tagged GTPases. Arrows denote areas of colocalization at the plasma membrane.

(B) Summary of plasma membrane recruitment analysis of the FHOD1-GBD by the indicated GTPases. The efficiency of GBD recruitment is indicated as "++" (in >90% of cells analyzed), "+" (recruitment in >50% of cells analyzed), "+/–" (recruitment in >30% of all cells analyzed), and "–" (undetectable recruitment).

(C) Isothermal titration calorimetry of FHOD1-GBD (P41K) with GST-Ras•GppNHp. The change in heating power indicated a specific interaction of activated Ras with the GBD mutant protein corresponding to a K_d value of 1.8 μM.

(D) ITC of FHOD1-GBD (P41K) with GST-Ras•GDP showed no interaction.

B

Rho-GTPases	
HA.Cdc42-G12V	–
HA.Cdc42 placental isoform G12V	+/–
HA.Rac1-G12V	++
HA.Rac2-G12V	++
HA.Rac3-G12V	+
HA.RhoA-G14V	–
HA.RhoB-G14V	–
HA.RhoC-G14V	–
Rho6/Rnd1	+/–
Rho7/Rnd2	+/–
Rho8/RhoE/Rnd3	+/–
RhoD/RhoHP1	–
RhoG	–
RhoH/TTF	–
TC10	–
TCL	+/–
Ras-GTPases	
HA.Rap1A-G12V	–
HA.Rap1B-G12V	–
HA.H-Ras-G12V	–
HA.K-Ras2-G12V	–
HA.M-Ras-G22V	–
HA.N-Ras-G12V	+/–
HA.R-Ras-G38V	+/–
Rap2A	–
Rap2B	–
Ras-like GTPases	
AGS1	–
RALA	–
RALB	–
RHEB2	–
RIG	–
RIT	–
RIT2	–
TC21	–

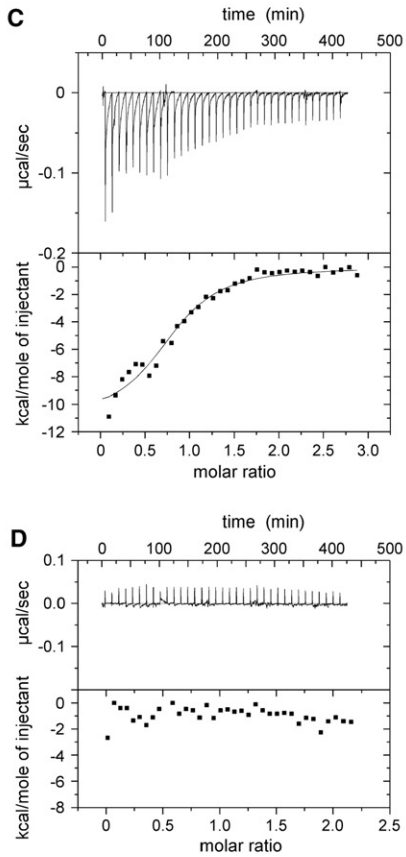

fold due to an unusual long loop in the GBD between β strands β1 and β2. The two domains are intimately connected by a short linker composed of only one residue (Q115). Additionally, a hydrophobic residue within the unique loop of the GBD, F29, inserts into the distal site of the first repeat of the FH3 domain structure, to tightly connect the domains.

Although sequence similarity between various Diaphanous-related formins is low and beyond unambiguous structural and functional generalization, the presence of an armadillo repeat structure in FHOD1 as the FH3-recognition domain for the DAD-autoregulatory motif establishes this fold as a conserved feature of DRFs. Residues on the concave surface of the second and third armadillo repeats that were found to mediate the interaction with the DAD in mDia1 (Lammers et al., 2005; Nezami et al., 2006) are not conserved in FHOD1 (Figure 2B), although the DAD consensus motif MDxLL is (Schönichen et al., 2006). However, a single point mutation V228E in the FH3 domain that was derived from the structural similarity to mDia1 potently activates FHOD1 in cells, presumably due to the disruption of the interaction surface to the autoregulatory DAD motif. FH3-DAD interactions therefore appear to operate according to one common structural principle shared across different DRF family members.

One marked difference in the structures of the N-terminal domains of FHOD1 and mDia1 is that $FHOD1_N$ appears not to be dimeric. In mDia1, the outgoing third helix of the fifth armadillo repeat seamlessly continues to a long interdomain helix that is followed by a dimerization subdomain composed of three interlaced helices (Otomo et al., 2005b; Rose et al., 2005). This assembly leads to the formation of a dimer interface in the N-terminal section of the formin besides the central FH2 domain which forms a head-to-tail dimer that clasps around the growing actin filament (Xu et al., 2004; Otomo et al., 2005a). For FHOD1, we could not observe a similar dimerization seed in the N-terminal domains. The sequence 340–377 following the FH3 domain is

highly polar and charged in FHOD1 (Figure 2B). A high content of charged residues in combination with multiple serine, threonine, and proline residues is typically associated with intrinsically unstructured protein domains. Crystals of elongated FHOD1 constructs (Figure S1B) all grow under conditions similar to those for 1–339 and displayed the same space group and identical unit-cell parameters. Also, size-exclusion chromatography showed a monomeric elution profile for the 1–377 fragment under reducing conditions (Schönichen et al., 2006). We thus assume that in contrast to Diaphanous family formins, the armadillo repeat structure of FHOD1 is followed by a polar, flexible linker section of at least 30 residues. The adjacent region 377–573 preceding the FH1 domain, however, might contain such a dimer interface and rebuild the topological similarity to mDia1.

The structure of the FHOD1 N terminus provides only the second domain organization of a formin GBD solved to date and reveals surprisingly pronounced differences to the mDia1-GBD. Based on this structural plasticity, the question arises whether any prediction can be made for GBDs of other DRF family members. Site-by-site comparisons between Dia and FHOD protein sequences to other DRFs suggested that the DAAM, FRL/FMNL, and FMN subfamilies likely contain an N-terminal GBD subdomain similar to mDia1. Inverted formin INF, so named because of the sequential inversion of catalytic and regulatory domains, does not show homology to any of the two GBD sequences. Delphilin, finally, contains a PDZ domain instead of the functional GBD-FH3 unit. FHOD proteins might thus be the only DRFs that contain a ubiquitin-like GTPase-binding domain for its activation. These suggestions are in line with previous phylogenetic analyses of GBD/FH3 domains which showed that FHOD sequences are most distant from any other DRF family (Rivero et al., 2005).

Our functional analyses suggest that the differences on the structural level translate into a role of the GBD in FHOD1 that is distinct from other DRFs. Whereas deletion of the GBD typically releases DRF autoinhibition similar to deletion of the DAD (Watanabe et al., 1999), FHOD1 variants lacking the N-terminal GBD were inactive. Importantly, this occurred even in the context of proposed constitutively active FHOD1 variants. The stability of these truncated FHOD1 proteins as well as the marked transition between GBD and FH3 subdomains suggest that this loss of function was not the result of structure destabilization. These observations would suggest that the N-terminal GBD plays roles in FHOD1 function beyond autoregulation.

It has recently been shown that phosphorylation of serine and threonine residues in the C-terminal DAD by ROCK is required for full activation of FHOD1 (Takeya et al., 2008). This result is in line with our structural observation that the proposed interaction sites on the bipartite unit of the GBD and FH3 domain for GTPases and DAD do not suggest a mechanism of displacement for the release of the inactive state. The presence of the GBD could thus be required for the recruitment of ROCK. On a speculative level, one could envision that binding of a GTPase to the GBD leads to conformational changes in the loop between β1 and β2, driven, for example, by ionic interactions of arginines R38 and R39 (see Figure S4). F29 could thus be displaced to open a hydrophobic groove in the FH3 domain and facilitate structural rearrangements or commit novel interactions. We therefore speculate that binding of the GBD to GTPases and possible other factors may facilitate FHOD's biological activity. Based on the GTPase-recruitment analysis presented, we favor the hypothesis that such interactions are critically involved in determining the subcellular localization of FHOD1. In line with such a scenario, coexpression of active Rac recruits FHOD1 to the plasma membrane (Gasteier et al., 2003; Koka et al., 2003). However, this relocalization does not induce actin-remodeling activity as observed upon experimental disruption of FH3-DAD autoinhibition. Additional, yet to be determined cofactors may thus be required to complement the DRF-GTPase complex for full activation. Future studies will be designed to address this hypothesis.

EXPERIMENTAL PROCEDURES

Protein Expression and Purification

The coding sequence of the N-terminal region of human FHOD1 was amplified by PCR from the full-length *fhod1* gene (NCBI GenBank accession number AF113615). Site-directed mutagenesis was performed using the mega primer method similarly as described (Schulte et al., 2005). All expression plasmids were confirmed by DNA sequencing prior to expression. Native and seleno-L-methionine-labeled $FHOD1_N$ proteins were produced in *Escherichia coli* cells and purified using Ni-NTA chromatography as described recently (Schulte et al., 2007). For crystallization, proteins were dialyzed in 20 mM Tris-HCl buffer (pH 7.6), 150 mM NaCl, 1 mM DTE, and concentrated to 20 mg/ml. Of note, expression of the sole FH3 domain (115–339) or mutant $FHOD1_N$(F29G) resulted in insoluble protein products.

GTPases of the Rho/Rac and Ras family were expressed from *E. coli* either as full-length constructs or C-terminally truncated to omit the membrane-binding anchor. H-Ras(1–189), H-Ras′(1–166), Rnd3′(16–200), TCL′(12–196), RhoA(1–193), Rac1(1–192), and Rac1′(1–179) were dialyzed against ITC buffer and typically concentrated to 10 mg/ml. Nucleotide exchange was performed as described (Geyer et al., 1996).

Crystallization, Structure Determination, and Refinement

Crystallization of $FHOD1_N$ as well as X-ray diffraction data collection are described elsewhere (Schulte et al., 2007). Data sets were collected from cryoprotected frozen crystals using a synchrotron radiation source. The structure of $FHOD1_N$ was determined by MAD phasing using data collected at two wavelengths (peak and inflection point). The positions of six (out of ten possible) selenium atoms in the asymmetric unit with two protein molecules were found using SHELXD (Schneider and Sheldrick, 2002). Heavy-atom position refinement and phasing were performed in CNS (Brunger et al., 1998) with the subsequent density modification procedure. The resulting electron density map clearly reflected the protein secondary structure element arrangement allowing the protein model building. Several rounds of model building in O (Jones et al., 1991) were followed by simulated annealing refinement using the Hendrickson-Lattman coefficient maximum likelihood as the refinement target in CNS. The final refinement runs (including simulated annealing, energy minimization, and B factor refinement) were performed using the structure factor maximum likelihood target in CNS with the native data set. The quality of the structural model and its agreement with the structure factors were checked with the program PROCHECK (Laskowski et al., 1993). Data quality and refinement statistics are given in Table 1. Superposition and rmsd value calculations were done with the program Coot (Krissinel and Henrick, 2004). The molecular diagrams were drawn using PyMOL (http://pymol.sourceforge.net/).

Isothermal Titration Calorimetry Binding Assays

Thermodynamic parameters of the $FHOD1_N$-GTPase interaction were determined by calorimetry (MCS-ITC; MicroCal). Proteins were dialyzed against ITC buffer (50 mM Tris-HCl [pH 7.5], 100 mM NaCl, 2 mM $MgCl_2$, 0.5 mM TCEP). H-Ras, Rnd3, TCL, RhoA, or Rac1 GTPases loaded with GppNHp or GDP were thermostated at concentrations of 20–50 μM in the sample cell at 15°C. $FHOD1_N$, FHOD1-GBD, and mutants thereof at 10-fold higher concentrations were injected stepwise into solution by volumes of 8 μl from a syringe. Changes in heating power were observed for 12 min until equilibrium was reached before the next injection was started. Data evaluation was performed using the manufacturer's analysis software, yielding ΔG° and ΔH° values with

typical errors of ±0.3 kcal/mol and dissociation constants with typical errors of ±0.15 μM. ITC experiments were repeated at least two times.

Mammalian Expression Constructs

The FHOD1 fragments coding for amino acids 1–115, 1–339, and 116–1164 were amplified by PCR from a wild-type FHOD1 expression construct (Gasteier et al., 2003). Forward and reverse primers were designed containing 5′ AflIII and 3′ EcoRI restriction sites, respectively. The FHOD1 fragment coding for the amino acids 116–1010 was amplified by PCR from a ΔC(1–1010) FHOD1 construct (Gasteier et al., 2003). The FHOD1 fragment 116–1164(DR9) was amplified by PCR from the FHOD1-DR9 construct (Schönichen et al., 2006). AflIII/EcoRI-digested PCR fragments were ligated into the NcoI/EcoRI sites of the pEF-HA or pEF-Myc expression vector, respectively. The V228E mutation was introduced by quick change PCR into the wt HA-FHOD1 construct using the QuikChange II XL site-directed mutagenesis kit (Stratagene). All plasmids were verified by sequencing. The GTPase-encoding expression constructs were purchased from the UMR cDNA Resource Center (http://www.cdna.org/).

Transfections and Immunofluorescence Microscopy

Functional analyses of FHOD1 proteins were carried out in NIH 3T3 cells essentially as described (Schönichen et al., 2006). For immunofluorescence, cells were plated onto glass coverslips overnight and subsequently transfected with a total of 4 μg DNA using Lipofectamine 2000 (Invitrogen). Twenty-four hours posttransfection, the cells were fixed with 3% paraformaldehyde (15 min at room temperature), permeabilized with PBS/0.1% Triton X-100 for 2 min, and blocked with PBS/1% BSA for 30 min. HA-tagged FHOD1 proteins and HA-tagged Rho-GTPases were revealed by staining with the rabbit polyclonal antibody Y-11 (Santa Cruz) and appropriate secondary antibodies conjugated with Alexa 568 and 488 (Molecular Probes), respectively. Cells were stained for F-actin using FITC-conjugated phalloidin (Sigma). Myc-tagged FHOD1 proteins were stained with the mouse monoclonal antibody 9E10 (Santa Cruz) and a secondary goat anti-mouse antibody conjugated to Alexa 568. Following extensive washing, cells were mounted with Mowiol (Calbiochem). Indirect fluorescence images were recorded either with an Olympus IX70 microscope or a Zeiss LSM Axiovert confocal microscope and processed using Adobe Photoshop.

SRE Transcription Assay

Activation of the SRE by FHOD1 was quantified in NIH 3T3 cells as previously described (Gasteier et al., 2003). Briefly, luciferase activity of starved NIH 3T3 cells was determined 48 hr postcotransfection of FHOD1 expression vectors, the 5×SRE-Luc reporter plasmid and pTK-Renilla, using a Luminoskan Ascent luminometer (Thermo Laboratories) and the dual luciferase reporter assay system kit (Promega). SRE firefly luciferase counts were normalized to the activity of the renilla luciferase internal control and calculated as fold transactivation with the counts for FHOD1-wt arbitrarily set to 1.

ACCESSION NUMBERS

The atomic coordinates and structure factors of $FHOD1_N$ have been deposited in the Protein Data Bank under ID code 3DAD.

SUPPLEMENTAL DATA

Supplemental Data include four figures and can be found with this article online at http://www.structure.org/cgi/content/full/16/9/1313/DC1/.

ACKNOWLEDGMENTS

We thank Diana Ludwig and Nadine Tibroni for expert technical assistance and I. Vetter, I. Schlichting, W. Blankenfeldt, N. Schrader, and M. Weyand for crystal diffraction data collection at the Swiss Light Source, Villigen. M.G. thanks Roger Goody for continuous support and stimulating discussions. O.P. and A.R. are supported by funds from the European Young Investigator (EURYI) award, DFG grant RA 1364/1-1, and the EC Sixth Framework Programme. This work was supported by a grant from the Deutsche Forschungsgemeinschaft to M.G. (GE 976/4) and O.T.F. (FA 378/6), and a fellowship GRK 1188 to B.S.

Received: May 30, 2008
Revised: May 30, 2008
Accepted: June 5, 2008
Published: September 9, 2008

REFERENCES

Alberts, A.S. (2001). Identification of a carboxyl-terminal Diaphanous-related formin homology protein autoregulatory domain. J. Biol. Chem. *276*, 2824–2830.

Andrade, M.A., Petosa, C., O'Donodhue, S.I., Müller, C.W., and Bork, P. (2001). Comparison of ARM and HEAT protein repeats. J. Mol. Biol. *309*, 1–18.

Brandt, D.T., Marion, S., Griffiths, G., Watanabe, T., Kaibuchi, K., and Grosse, R. (2007). Dia1 and IQGAP1 interact in cell migration and phagocytic cup formation. J. Cell Biol. *178*, 193–200.

Brunger, A.T., Adams, P.D., Clore, G.M., DeLano, W.L., Gros, P., Grosse-Kunstleve, R.W., Jiang, J.S., Kuszewski, J., Nilges, M., Pannu, N.S., et al. (1998). Crystallography & NMR system: a new software suite for macromolecular structure determination. Acta Crystallogr. D Biol. Crystallogr. *54*, 905–921.

Conti, E., Uy, M., Leighton, L., Blobel, G., and Kuriyan, J. (1998). Crystallographic analysis of the recognition of a nuclear localization signal by the nuclear import factor karyopherin α. Cell *94*, 193–204.

Evangelista, M., Zigmond, S., and Boone, C. (2003). Formins: signaling effectors for assembly and polarization of actin filaments. J. Cell Sci. *116*, 2603–2611.

Faix, J., and Grosse, R. (2006). Staying in shape with formins. Dev. Cell *10*, 693–706.

Gasteier, J.E., Madrid, R., Krautkramer, E., Schroder, S., Muranyi, W., Benichou, S., and Fackler, O.T. (2003). Activation of the Rac-binding partner FHOD1 induces actin stress fibers via a ROCK-dependent mechanism. J. Biol. Chem. *278*, 38902–38912.

Geyer, M., and Wittinghofer, A. (1997). GEFs, GAPs, GDIs and effectors: taking a closer (3D) look at the regulation of Ras-related GTP-binding proteins. Curr. Opin. Struct. Biol. *7*, 786–792.

Geyer, M., Schweins, T., Herrmann, C., Prisner, T., Wittinghofer, A., and Kalbitzer, H.R. (1996). Conformational transitions in p21ras and in its complexes with the effector protein Raf-RBD and the GTPase activating protein GAP. Biochemistry *35*, 10308–10320.

Geyer, M., Herrmann, C., Wohlgemuth, S., Wittinghofer, A., and Kalbitzer, H.R. (1997). Structure of the Ras-binding domain of RalGEF and implications for Ras binding and signalling. Nat. Struct. Biol. *4*, 694–699.

Goode, B.L., and Eck, M.J. (2007). Mechanism and function of formins in control of actin assembly. Annu. Rev. Biochem. *76*, 593–627.

Herrmann, C. (2003). Ras-effector interactions: after one decade. Curr. Opin. Struct. Biol. *13*, 122–129.

Higashida, C., Miyoshi, T., Fujita, A., Oceguera-Yanez, F., Monypenny, J., Andou, Y., Narumiya, S., and Watanabe, N. (2004). Actin polymerization-driven molecular movement of mDia1 in living cells. Science *303*, 2007–2010.

Higgs, H.N., and Peterson, K.J. (2005). Phylogenetic analysis of the formin homology 2 domain. Mol. Biol. Cell *16*, 1–13.

Huang, L., Hofer, F., Martin, G.S., and Kim, S.H. (1998). Structural basis for the interaction of Ras with RalGDS. Nat. Struct. Biol. *5*, 422–426.

Ishizaki, T., Morishima, Y., Okamoto, M., Furuyashiki, T., Kato, T., and Narumiya, S. (2001). Coordination of microtubules and the actin cytoskeleton by the Rho effector mDia1. Nat. Cell Biol. *3*, 8–14.

Jones, T.A., Zou, J.Y., Cowan, S.W., and Kjeldgaard, M. (1991). Improved methods for building protein models in electron density maps and the location of errors in these models. Acta Crystallogr. A *47*, 110–119.

Kato, T., Watanabe, N., Morishima, Y., Fujita, A., Ishizaki, T., and Narumiya, S. (2001). Localization of a mammalian homolog of diaphanous, mDia1, to the mitotic spindle in HeLa cells. J. Cell Sci. *114*, 775–784.

Kiel, C., and Serrano, L. (2006). The ubiquitin domain superfold: structure-based sequence alignments and characterization of binding epitopes. J. Mol. Biol. *355*, 821–844.

Koka, S., Neudauer, C.L., Li, X., Lewis, R.E., McCarthy, J.B., and Westendorf, J.J. (2003). The formin-homology-domain-containing protein FHOD1 enhances cell migration. J. Cell Sci. *116*, 1745–1755.

Krissinel, E., and Henrick, K. (2004). Secondary-structure matching (SSM), a new tool for fast protein structure alignment in three dimensions. Acta Crystallogr. D Biol. Crystallogr. *60*, 2256–2268.

Lammers, M., Rose, R., Scrima, A., and Wittinghofer, A. (2005). The regulation of mDia1 by autoinhibition and its release by Rho*GTP. EMBO J. *24*, 4176–4187.

Laskowski, R.A., MacArthur, M.W., Moss, D.S., and Thornton, J.M. (1993). PROCHECK: a program to check the stereochemical quality of protein structures. J. Appl. Crystallogr. *26*, 283–291.

Li, F., and Higgs, H.N. (2005). Dissecting requirements for auto-inhibition of actin nucleation by the formin, mDia1. J. Biol. Chem. *280*, 6986–6992.

Lu, J., Meng, W., Poy, F., Maiti, S., Goode, B.L., and Eck, M.J. (2007). Structure of the FH2 domain of Daam1: implications for formin regulation of actin assembly. J. Mol. Biol. *369*, 1258–1269.

Madrid, R., Gasteier, J.E., Bouchet, J., Schroder, S., Geyer, M., Benichou, S., and Fackler, O.T. (2005). Oligomerization of the diaphanous-related formin FHOD1 requires a coiled-coil motif critical for its cytoskeletal and transcriptional activities. FEBS Lett. *579*, 441–448.

Nassar, N., Horn, G., Herrmann, C., Scherer, A., McCormick, F., and Wittinghofer, A. (1995). The 2.2 Å crystal structure of the Ras-binding domain of the serine/threonine kinase c-Raf1 in complex with Rap1A and a GTP analogue. Nature *375*, 554–560.

Nezami, A.G., Poy, F., and Eck, M.J. (2006). Structure of the autoinhibitory switch in formin mDia1. Structure *14*, 257–263.

Orengo, C.A., Michie, A.D., Jones, S., Jones, D.T., Swindells, M.B., and Thornton, J.M. (1997). CATH—a hierarchic classification of protein domain structures. Structure *5*, 1093–1108.

Otomo, T., Tomchick, D.R., Otomo, C., Panchal, S.C., Machius, M., and Rosen, M.K. (2005a). Structural basis of actin filament nucleation and processive capping by a formin homology 2 domain. Nature *433*, 488–494.

Otomo, T., Otomo, C., Tomchick, D.R., Machius, M., and Rosen, M.K. (2005b). Structural basis of Rho GTPase-mediated activation of the formin mDia1. Mol. Cell *18*, 273–281.

Ozaki-Kuroda, K., Yamamoto, Y., Nohara, H., Kinoshita, M., Fujiwara, T., Irie, K., and Takai, Y. (2001). Dynamic localization and function of Bni1p at the sites of directed growth in *Saccharomyces cerevisiae*. Mol. Cell. Biol. *21*, 827–839.

Pacold, M.E., Suire, S., Perisic, O., Lara-Gonzalez, S., Davis, C.T., Walker, E.H., Hawkins, P.T., Stephens, L., Eccleston, J.F., and Williams, R.L. (2000). Crystal structure and functional analysis of Ras binding to its effector phosphoinositide 3-kinase γ. Cell *103*, 931–943.

Pantaloni, D., Le Clainche, C., and Carlier, M.F. (2001). Mechanism of actin-based motility. Science *292*, 1502–1506.

Pearson, M.A., Reczek, D., Bretscher, A., and Karplus, P.A. (2000). Structure of the ERM protein moesin reveals the FERM domain fold masked by an extended actin binding tail domain. Cell *101*, 259–270.

Petersen, J., Nielsen, O., Egel, R., and Hagan, I.M. (1998). FH3, a domain found in formins, targets the fission yeast formin Fus1 to the projection tip during conjugation. J. Cell Biol. *141*, 1217–1228.

Pollard, T.D., and Borisy, G.G. (2003). Cellular motility driven by assembly and disassembly of actin filaments. Cell *112*, 453–465.

Pruyne, D., Evangelista, M., Yang, C., Bi, E., Zigmond, S., Bretscher, A., and Boone, C. (2002). Role of formins in actin assembly: nucleation and barbed-end association. Science *297*, 612–615.

Rivero, F., Muramoto, T., Meyer, A.K., Urushihara, H., Uyeda, T.Q., and Kitayama, C. (2005). A comparative sequence analysis reveals a common GBD/FH3-FH1-FH2-DAD architecture in formins from *Dictyostelium*, fungi and metazoa. BMC Genomics *6*, 28.

Romero, S., Le Clainche, C., Didry, D., Egile, C., Pantaloni, D., and Carlier, M.F. (2004). Formin is a processive motor that requires profilin to accelerate actin assembly and associated ATP hydrolysis. Cell *119*, 419–429.

Rose, R., Weyand, M., Lammers, M., Ishizaki, T., Ahmadian, M.R., and Wittinghofer, A. (2005). Structural and mechanistic insights into the interaction between Rho and mammalian Dia. Nature *435*, 513–518.

Sagot, I., Rodal, A.A., Moseley, J., Goode, B.L., and Pellman, D. (2002). An actin nucleation mechanism mediated by Bni1 and profilin. Nat. Cell Biol. *4*, 626–631.

Scheffzek, K., Grunewald, P., Wohlgemuth, S., Kabsch, W., Tu, H., Wigler, M., Wittinghofer, A., and Herrmann, C. (2001). The Ras-Byr2RBD complex: structural basis for Ras effector recognition in yeast. Structure *9*, 1043–1050.

Schneider, T.R., and Sheldrick, G.M. (2002). Substructure solution with SHELXD. Acta Crystallogr. D Biol. Crystallogr. *58*, 1772–1779.

Schönichen, A., Alexander, M., Gasteier, J.E., Cuesta, F.E., Fackler, O.T., and Geyer, M. (2006). Biochemical characterization of the diaphanous autoregulatory interaction in the formin homology protein FHOD1. J. Biol. Chem. *281*, 5084–5093.

Schulte, A., Czudnochowski, N., Barboric, M., Schonichen, A., Blazek, D., Peterlin, B.M., and Geyer, M. (2005). Identification of a cyclin T-binding domain in Hexim1 and biochemical analysis of its binding competition with HIV-1 Tat. J. Biol. Chem. *280*, 24968–24977.

Schulte, A., Rak, A., Pylypenko, O., Ludwig, D., and Geyer, M. (2007). Purification, crystallization and preliminary structural characterization of the N-terminal region of the human formin-homology protein FHOD1. Acta Crystallogr. Sect. F Struct. Biol. Cryst. Commun. *63*, 878–881.

Seth, A., Otomo, C., and Rosen, M.K. (2006). Autoinhibition regulates cellular localization and actin assembly activity of the diaphanous-related formins FRLα and mDia1. J. Cell Biol. *174*, 701–713.

Shimada, A., Nyitrai, M., Vetter, I.R., Kuhlmann, D., Bugyi, B., Narumiya, S., Geeves, M.A., and Wittinghofer, A. (2004). The core FH2 domain of diaphanous-related formins is an elongated actin binding protein that inhibits polymerization. Mol. Cell *13*, 511–522.

Takeya, R., and Sumimoto, H. (2003). Fhos, a mammalian formin, directly binds to F-actin via a region N-terminal to the FH1 domain and forms a homotypic complex via the FH2 domain to promote actin fiber formation. J. Cell Sci. *116*, 4567–4575.

Takeya, R., Taniguchi, K., Narumiya, S., and Sumimoto, H. (2008). The mammalian formin FHOD1 is activated through phosphorylation by ROCK and mediates thrombin-induced stress fibre formation in endothelial cells. EMBO J. *27*, 618–628.

Vavylonis, D., Kovar, D.R., O'Shaughnessy, B., and Pollard, T.D. (2006). Model of formin-associated actin filament elongation. Mol. Cell *21*, 455–466.

Vetter, I.R., Linnemann, T., Wohlgemuth, S., Geyer, M., Kalbitzer, H.R., Herrmann, C., and Wittinghofer, A. (1999). Structural and biochemical analysis of Ras-effector signaling via RalGDS. FEBS Lett. *451*, 175–180.

Wallar, B.J., and Alberts, A.S. (2003). The formins: active scaffolds that remodel the cytoskeleton. Trends Cell Biol. *13*, 435–446.

Watanabe, N., Kato, T., Fujita, A., Ishizaki, T., and Narumiya, S. (1999). Cooperation between mDia1 and ROCK in Rho-induced actin reorganization. Nat. Cell Biol. *1*, 136–143.

Westendorf, J.J. (2001). The formin/diaphanous-related protein, FHOS, interacts with Rac1 and activates transcription from the serum response element. J. Biol. Chem. *276*, 46453–46459.

Westendorf, J.J., Mernaugh, R., and Hiebert, S.W. (1999). Identification and characterization of a protein containing formin homology (FH1/FH2) domains. Gene *232*, 173–182.

Wohlgemuth, S., Kiel, C., Kramer, A., Serrano, L., Wittinghofer, A., and Herrmann, C. (2005). Recognizing and defining true Ras binding domains I: biochemical analysis. J. Mol. Biol. *348*, 741–758.

Xu, Y., Moseley, J.B., Sagot, I., Poy, F., Pellman, D., Goode, B.L., and Eck, M.J. (2004). Crystal structures of a formin homology-2 domain reveal a tethered dimer architecture. Cell *116*, 711–723.